Design and simulation of a Banki cross-flow wind turbine for highways under high turbulence and high altitude conditions

Eduard Matheo Alave-Vargas[a], Valentina Rita Villarroel-Beltrán[a], Renán Orelllana Lafuente[a], Cecilia Tapia-Siles[b] and Daniel Felipe Sempértegui-Tapia[a]

[a] Laboratorio de Energías Alternativas, Centro de Investigaciones Ópticas y Energía, Universidad Privada Boliviana, Cochabamba, Bolivia, dsempertegui@upb.edu, CA
[b] Laboratorio de Innovación Tecnológica Industrial y Robótica, Universidad Privada Boliviana, Cochabamba, Bolivia.

Abstract:

The objective of this study is to design an optimal vertical axis wind turbine (VAWT) for electric generation on a high-density urban highway in Cochabamba, Bolivia, taking into account the special functional conditions due to the characteristics of the high altitude area. Based on the literature, it was initially determined that the Banki cross-flow turbine is the most suitable VAWT for use on highways. An in-situ measurement of the wind velocity spectra was conducted to assess the typical wind characteristics along the highway using statistical analysis and selected optimal values for testing and optimization. The diameter of the Banki wind turbine was then determined and fixed considering the width of the space between the two lanes of the highway as a limitation. Three geometrical aspects were assessed as variables for finding the optimal power coefficient; attack angle, number of blades and height. Computational fluid dynamics (CFD) simulations were carried out with every turbine combination to determine the optimal characteristics. From C_p and TSR values obtained from the simulations a multivariate analysis was carried out optimizing these values. The response of C_p and TSR were obtained, prioritizing C_p results. Finally, an ultimate design for the Banki wind turbine is proposed. The optimized Banki cross flow turbine has 11.5495° attack angle, 12 number of blades and 0.9 m of height.

Keywords: Vertical Axis Wind Turbine, Energy harvesting, Highway wind turbine, Banki Cross-flow

1. Introduction

Nowadays, the world is facing an energy crisis resulting from a shortage of traditional energy resources. As a result, many countries have started to shift their focus towards renewable energy alternatives such as solar thermal and photovoltaic energy, hydro energy, geothermal energy and wind energy to generate power.

Recent technological advances and diversification of types of wind turbines show a reduction in the risk of these installations and present more efficient systems in electrical conversion. Nevertheless, wind energy generation has shown to be a risky investment for the development of an interconnected power grid due to wind energy variability and uncertainty, its effect on power fluctuations, voltage drops, and as a consequence, grid instability.

The trend within wind turbines falls on a horizontal configuration of their axes or HAWT (horizontal axis wind turbine), mainly due to their large generation capacities within a specific area. However, horizontal-axis wind turbines are complex projects that cannot compete in micro-scale markets due to demanding operating conditions, large investments and studies, and high maintenance costs. A more relegated but no less important technology is the vertical axis wind turbine or VAWT (vertical axis wind turbine), which has an increased demand due to the need to take advantage of resources in limited environments. These turbines allow easy integration into the market of products for electricity generation and installation in urban areas for micro-generation and self-sustainability of products. The VAWT stands out due to the possibility of self-starting the generation as well as the omnidirectional capacity to harvest winds; factors that are limiting for horizontal axis wind turbines. In addition, new studies consider the use of sets of VAWTs in different configurations to increase efficiency or new types of airfoils with the same purpose, taking advantage of fluid mechanics and phenomena occurring during their operation.

In the literature, the principal focus of the research on VAWTs is the geometrical design, consequently, the VAWTs are continually being adapted and redesigned to achieve maximum benefits in power generation. Geometrical design of a Nautilus wind turbine [1], a comparison between helical and straight blades [2] and a

nature-inspired shape blades proposal for a VAWT [3] are some examples. Likewise, VAWTs have been researched to suit specific applications, such as subsidized houses [4] and highways [5], [6]. On highways, the authors are exploring the possibility of using VAWTs for electricity generation and street lighting, with certain types of turbines, with the cross-flow Banki wind turbine appearing to be the most effective option. Recent developments have also focused on enhancing the efficiency of arrays of vertical wind turbines [6], [7], [8]. Moreover, wind deflectors or guiding vanes are being studied as a solution to the performance challenges of some turbines [9]. Additional details and discussion on the state-of-the-art of VAWTs can be found on a recent review done by Alave-Vargas et al. [10].

In this sense, the present article will propose the design of an optimal Banki-type vertical axis wind turbine according to specific wind conditions and data analysis of in-situ measurements of the location within Blanco Galindo highway in Cochabamba, Bolivia; a city that is located at 2558 m.a.s.l., which implies a high altitude condition that has effects on the viscosity and density of air. The experiment consists on the geometrical design based on the angle of attack, height, and the number of blades of the turbine. The experiment will be carried out on computational fluid dynamics (CFD) recording moment and angular velocity to perform an efficiency analysis, obtaining an optimal Banki wind turbine that can be used in-site.

2. Types of vertical axis wind turbines

Although horizontal axis wind turbines have been extensively studied and are currently used as the prime wind energy generation turbine in the world, new advances and studies have emerged related to the construction and application of vertical axis wind turbines and emphasize the optimal values of tip-speed ratio (TSR), power coefficient (C_p), thrust coefficient (C_t) and the cut-in speed at which the turbine starts generating [1].

The values of TSR for VAWTs are determined by the turbine geometry, installation conditions and required power output. TSR is defined as the relation between the blade tip velocity and the wind speed. A high TSR value means higher power output, but it can cause mechanical issues. The C_p measures the turbine's efficiency converting the kinetic energy of the wind into electrical energy, and its maximum value occurs at a specific TSR value. The calculation of C_p is defined by Eq. (1). The C_t also measures the efficiency of the turbine extracting energy from the wind, and depends on the thrust force produced by the turbine, air density, wind speed, and swept area of the turbine, this value is represented by Eq. (2). A high C_t value indicates higher efficiency, but it could cause the turbine to fail mechanically as suggested by [11] and [5].

$$C_p = \frac{P}{\frac{1}{2} \cdot \rho \cdot S \cdot V^3},$$

(1)

$$C_t = \frac{\tau}{\frac{1}{4} \cdot \rho \cdot S \cdot V^2 \cdot D_1},$$

(2)

The types of vertical axis wind turbines, according to recent literature, can be divided on:

2.1. Darrieus turbine

Darrieus rotors were invented in the third decade of the 20th century in France. They consist of 2 or 3 blades parallel to the axis of the rotor [12]. Regarding sub-types, there are Darrieus turbines with straight blades, with H rotor and with curved blades. They are considered the most efficient vertical-axis turbines [5], [6], and also very trustful [13].

The Darrieus turbines generate power from the lift produced by the rotating airfoils and have a higher power coefficient than the Savonius turbine [14]. They are recommended for use in areas with high and constant wind speeds without noticeable variations [15].

2.2. Savonius turbine

The Savonius turbine is used for variable wind flows in different ranges and requires a minimum wind speed to start working [15]. Despite being less efficient than the Darrieus turbines, it has been shown to have higher starting torque and good starting performance [5], [13].

2.3. Banki turbine

The Michell-Banki or Banki turbine is a cross-flow wind turbine type. Experiments have shown that it outperforms the Savonius and Darrieus vertical axis turbines in certain conditions and on highway applications [16]. It has a low autostart of around 1.2 m/s, relatively high torque and a rigid structure [13]. The remarkable efficiency of this turbine is due to the fact that the wind passes through two stages. In the first stage, the wind enters the turbine hitting the blades facing the wind and in the second stage, it leaves the turbine hitting the blades facing backwards. A large number of blades gives the turbine the ability to have low connection speed and high starting torque [11].

The construction of Banki turbines adapted for wind applications can be designed following a series of guidelines and equations, proposed by Al-Maaitah [11]. They define the maximum efficiency or C_p of the turbine

for the given context, where the geometry of the exposed blades is specifically designed using a velocity triangle as shown in Figure 1.
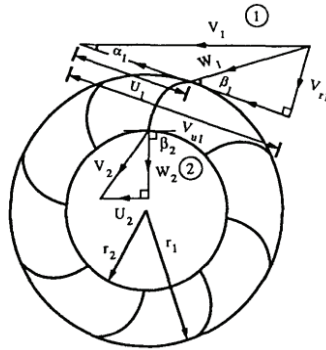

Figure. 1. *Velocity triangle diagram of wind input and output of the rotor* [11].

Through a geometric analysis of the velocity triangles of the input speed (system 1) and the output speed (system 2), Eq. (3) and Eq. (4) are obtained, where r_2 corresponds to the inner radius, r_1 is the outer radius, α_1 represents the angle of attack, and β_1 represent the input blade angle.

$$\left(\frac{r_2}{r_1}\right)^4 + 4 \cdot \left(\frac{r_2}{r_1}\right)^2 \cdot tan^2(\alpha_1) - tan^2(\alpha_1) = 0, \tag{3}$$

$$tan\,\beta_1 = 2 \cdot tan\,\alpha_1, \tag{4}$$

With the definition of the radius, Sammartano et al. [17] proposed the Eq. (5) and Eq. (6) to calculate the radius of curvature of ρ_b and degree of curvature of the blade δ, this geometry is shown in Figure 2.

$$\rho_b = \frac{D_1}{4} \cdot \left[1 - \left(\frac{D_2}{D_1}\right)^2\right] \cdot cos\,(\beta_1)^{-1}, \tag{5}$$

$$tan\left(\frac{\delta}{2}\right) = \frac{cos(\beta_1)}{sin(\beta_1)}, \tag{6}$$
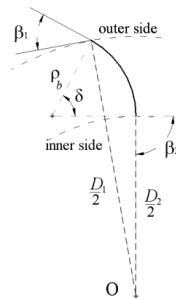

Figure. 2. *Blade geometry* [17].

3. In-site wind resource analysis

In order to carry out a design based on real conditions, wind speed measurements were taken on the Blanco Galindo highway in the city of Cochabamba, Bolivia. This avenue has a double lane with one lane going east and the other going west, and a space of 1.86 m separating the lanes of opposite circulation.

The data collection was carried out at 3.5 km of the highway, 460 metres from the distributor of another important avenue, Beijing avenue (the exact location can be seen in Figure 3). The criteria for determining the location for data collection were based on the observation of high vehicular flow, circulation of trucks and heavy vehicles coming from the distributor, and the absence of traffic lights within a radius of at least 400 metres.
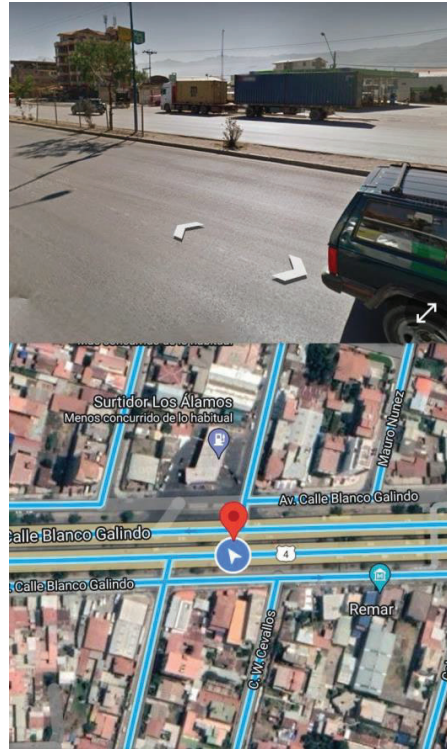
Figure. 3. Location of the data gathering point (-17.393004, -66.188506).

Wind data were collected for four days at different periods, taking into account high traffic periods caused by rush hours. During the measurement days, there was no rain or significant variations in temperature and humidity. Anemometers with data loggers and Bluetooth were used with a collection frequency of 1 data/s. The data was measured at 1 m from the ground; this selection is based on a study by Al-Aqel et al. [18]. They concluded that the maximum recorded wind speed is found at that height because of the formation of trailing vortices behind and at the sides of vehicles. The results obtained for periods, in terms of maximum wind speeds and average speeds, are shown in Table 1.

Table 1. Summary of wind speed data.

Period	Day	From	To	Maximum wind velocity north side, m/s	Maximum wind velocity south side, m/s	Average wind speed north side, m/s	Average wind speed south side, m/s
Period 1	Wednesday	08:58 am	10:00 am	7.29	3.49	1.598	1.226
Period 2	Wednesday	11:47 am	12:55 pm	7.64	7.63	2.237	1.898
Period 3	Thursday	08:58 am	09:58 am	6.31	6.35	1.305	1.445
Period 4	Thursday	12:06 am	01:08 pm	5.94	4.42	1.806	0.655
Period 5	Friday	08:22 am	10:00 am	10.14	0.00	2.050	0.000
Period 6	Friday	12:04 pm	01:08 pm	9.47	4.42	2.180	0.655
Period 7	Friday	04:09 pm	05:01 pm	7.23	6.17	1.494	1.722
Period 8	Saturday	07:42 am	08:45 am	7.75	5.79	2.622	0.938

For a better understanding of the data, Table 2 presents the percentage of data that corresponds to a specific range of wind speed.

Table 2. Range wind speed percentage.

Wind speed range , m/s	Data percentage north side, %	Data percentage south side, %
0.1 - 1.1	27.20	57.58
1.2 - 2.1	41.01	27.52
2.2 - 3.1	19.97	12.26
3.2 - 5-1	7.920	2.540
5.2 - 10.2	3.900	0.100

As shown in Table 2, the entirety of the collected data is concentrated between 0.1 and 2.1 m/s, with at least 68% of the measurements on both sides falling within this range. There are some variations between the south and north side measurements, with higher values consistently recorded on the north side. However, while the data is consistent, the measured wind speeds are limited to specific periods and have a low magnitude, which limits their potential as a good wind resource [13], [18]. Therefore, for the purpose of obtaining an optimal turbine design, a higher wind speed value will be used. During the Saturday measurements, higher wind speeds were recorded on the north side, with every measurement greater than 5 m/s, with a mean value of 6.15 m/s. The first measured speed on the north side with this value has a 1.98 m/s speed on the south side. These two values were used for the development of all CFD simulations.

4. Experimental design

To obtain the most efficient turbine possible, a series of parameters and limitations must be defined. Since the turbine must be located in the middle of the highway and the maximum width is 1.86 m, the diameter will be limited to 1.4 m, taking into consideration safety factors to prevent risking human lives during its operation. Other considerations for the site include the local density and viscosity of the air, which were extracted from the EES software library, corresponding to the air pressure at 2,558 m.a.s.l. with a value of 0.8913 kg/m^3 and 1.82E-5 m^2/s, respectively. The experiment will not focus on power production and will analyse the optimal turbine with the dimensionless coefficient C$_p$. This parameter will enable the comparison of turbines with different configurations and give an idea of the raw power they can produce [5], [19], [20]. Since the experiment will be conducted on a double duct wind tunnel, the defined TSR concept will be adapted to consider wind speed as the sum of the speed in both lanes; C$_t$ and C$_p$ will have a similar variation using the sum of wind speeds as the parameter. Finally, a factorial statistical analysis will be carried out using the peak values obtained from the parameters of each turbine to obtain the optimal values for each turbine's geometrical parameters.

4.1. Turbine type selection

Many types of turbines have been studied, each with its advantages and disadvantages in different situations and wind characteristics. Highways have a wind resource that is not related to climate phenomena and has high turbulence and a mixture of air, as well as short bursts of air that require the use of low-starting torque turbines. Tian et al. [6] conducted a study comparing the Savonius, Darrieus, and Banki turbine designs for highway energy recovery applications. The results showed that the Banki wind turbine is the most efficient for energy production on a turbine situated on a highway due to its drag characteristics, which allow it to perform at low wind speeds and high torque. This is why in the current study, this turbine will be analysed and used for highway energy recovery.

Considering that there is an interest in building a functional prototype of the wind turbine, the material selection was carefully considered. While many authors utilize models with aluminium or composite materials, these materials can be both high-density and expensive. To mitigate these issues, a solid polyvinyl chloride (PVC) with a density of 1.4 g/cm³ was chosen for its ease at manufacturing, natural material resistance, low cost, and availability in the local Bolivian market. This choice of material allows for the turbine's geometrical properties to be easily constructed while still maintaining its functionality [21], [22], [23].

4.2. Geometric design parameters

After selecting the Banki wind turbine for simulation to find the geometric design parameters for the operating conditions, parameters such as height, angle of attack, and number of blades for Banki turbines with similar characteristics are presented. Tian et al. [6] used 18 blades, a radius of 0.25 m, and a height of 0.21 m for the Banki turbine design. Al-Maaitah [11] used an angle of attack of 16°, a height of 1 m, and 8 blades. However, Ushiyama et al. [24] suggest that the turbine must have a minimum of 12 blades to be more effective. Andrade et al. [25] have demonstrated through experiments that the angle of attack can vary from 7° to 23°. On the other hand, Sammartano et al. [17] use a design with 35 blades, an angle of attack of 22°, and a height of 1 m.

Based on these experiences, it was decided to establish three angles of attack (6°, 10°, and 14°), rotor heights of 0.9 m and 1.1 m, and numbers of blades of 12, 16, and 20. Therefore, 18 possible turbine designs were created. For all these combinations, calculations were made using the proposed equations for Banki turbine design. The outer radius r_1 was defined based on the available space of 1.86 m where wind speed measurements were taken, with a fixed value of 0.7 m. Equation (3) was used to calculate the inner radius r_2 and Eq. (4) to obtain the blade angle β_1. The geometric parameters that complete the blade geometry, the radius of curvature and the curvature angle, were calculated using Eq. (5) and Eq. (6). The geometrical design parameters are shown in Figure 4a and the computer model of a specific Banki turbine is illustrated in Figure 4b.
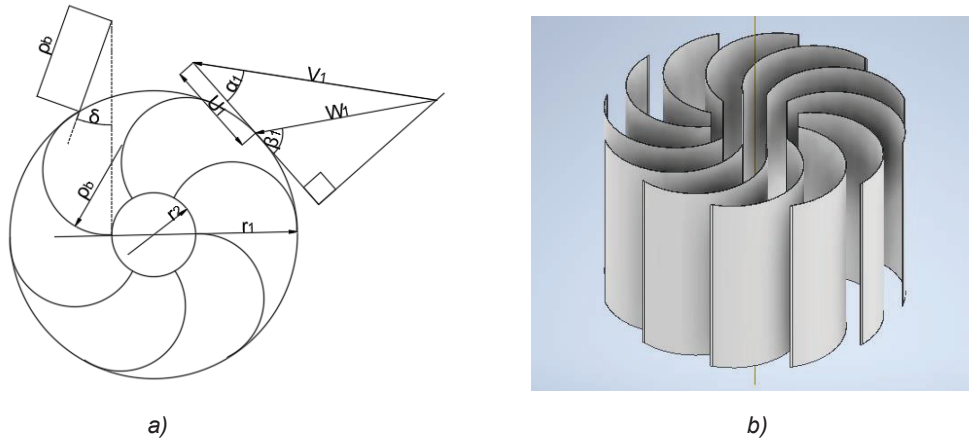
Figure. 4. *a) Geometric design parameters for a Banki wind turbine, b) 3D model of the Banki turbine.*

For the 18 turbines geometries, using 3D computer design software with the selected material, their mass and moment of inertia were obtained. These results for all possible combinations are presented in Table 3.

Table 3. *Design parameters.*

Part name	Angle of attack α_1	Number of blades	Height, cm	Blade angle β_1	Radius of curvature ρ_b, m	Degree of curvature δ	r_1, m	r_2, m	Mass turbine kg	Inertia moment kg m^2
TS-01	6°	12	90	11.87°	0.327	23.72°	0.7	0.204	32.543	8.8820
TS-02	6°	12	110	11.87°	0.327	23.72°	0.7	0.204	39.774	10.856
TS-03	6°	16	90	11.87°	0.327	23.72°	0.7	0.204	43.390	11.843
TS-04	6°	16	110	11.87°	0.327	23.72°	0.7	0.204	55.032	14.475
TS-05	6°	20	90	11.87°	0.327	23.72°	0.7	0.204	54.238	14.804
TS-06	6°	20	110	11.87°	0.327	23.72°	0.7	0.204	66.290	18.094
TS-07	10°	12	90	19.42°	0.325	38.85°	0.7	0.247	27.608	7.6210
TS-08	10°	12	110	19.42°	0.325	38.85°	0.7	0.247	33.743	9.3140
TS-09	10°	16	90	19.42°	0.325	38.85°	0.7	0.247	36.810	10.161
TS-10	10°	16	110	19.42°	0.325	38.85°	0.7	0.247	44.990	12.419
TS-11	10°	20	90	19.42°	0.325	38.85°	0.7	0.247	46.013	12.701
TS-12	10°	20	110	19.42°	0.325	38.85°	0.7	0.247	56.238	15.524
TS-13	14°	12	90	26.50°	0.330	53.00°	0.7	0.274	24.404	6.7910
TS-14	14°	12	110	26.50°	0.330	53.00°	0.7	0.274	29.827	8.3000
TS-15	14°	16	90	26.50°	0.330	53.00°	0.7	0.274	32.539	9.0550
TS-16	14°	16	110	26.50°	0.330	53.00°	0.7	0.274	39.769	11.067
TS-17	14°	20	90	26.50°	0.330	53.00°	0.7	0.274	40.673	11.318
TS-18	14°	20	110	26.50°	0.330	53.00°	0.7	0.274	49.712	13.833

With the 18 possibilities of wind turbines a multivariable analysis will be carried out. The study will analyse the influence of the angle of attack, number of blades, and height in power production; correlating these parameters to the C_p and TSR of the turbine. From this analysis, an optimal geometrically designed turbine will be obtained. Integer steps were proposed to evaluate a high number of transient analyses, covering a broad range of values. While smaller steps in all variables would increase the precision of the statistical analysis allowing us to reach more specific values, there are limitations to do it without increasing the length of the study.

4.3. Performance simulations

4.3.1. Numerical methods and computational domain

A CFD simulation has been conducted using Ansys Fluent. The numerical simulation was performed with a k - ε turbulence model due to its accuracy; the enhanced wall treatment condition was applied. The simulations used dynamic mesh and included the mass and inertia data from each turbine to generate the movement in the respective flow. A pressure-based solver was chosen and velocity inlets were defined, with inlet 1 having a value of 6.15 m/s and inlet 2 having a value of 1.98 m/s with their disposition shown in Figure 5. Both outlets were pressure based with a gauge pressure of 0 and assumed no loss [26].
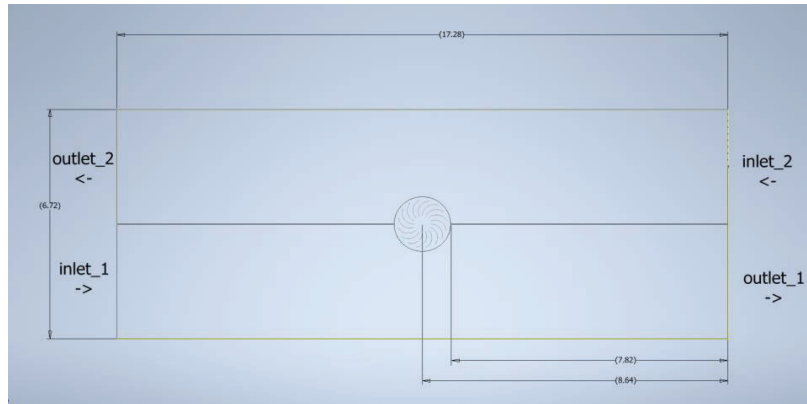
Figure. 5. *Computational domains for CFD simulations (dimensions are m).*

For the current analysis, the turbine was isolated from interaction with vehicles, and a separator in the middle was used for the flows to develop completely. This separator is a thin wall 20 mm thick, allowing the turbine to be analysed without mixing the flows and obtaining the optimal design based solely on performance under similar conditions to those on the highway, not including elevated turbulence of air. Creating an adequate computational domain is necessary to generate real results from the data input into the simulation. When the computational domain is too short, the flow does not resemble a real flow, and when it is too large, the duration of the computational process is considerably long [20]. The computational domains are analogous to Toudasrbari et al. [20], and consist of a rectangle of 17.28 m x 6.72 m. The values were decreased from other studies due to the crossflow characteristics of the domain as shown in Figure 5. The thin wall that separates both flows and avoids interaction between them before reaching the turbine is 7.82 m from the lateral wall, allowing a small gap that generates the resultant mixture of air due to the turbine interacting with the flow. The domain is 1.5 m tall since it is not necessary to analyse the flow in the y-axis.

4.3.2. Mesh generation and simulation setup

The meshing type and size are crucial in every CFD simulation to generate good results and accuracy. The meshing generation uses multizone generation for the wind turbine, where the resultant mesh has a free mesh type of tetrahedral elements and hexa/prism elements for the whole domain. As shown in Figure 6, the number of elements has a higher density over the turbine to correctly calculate the flow and to resemble a real one. On average, the whole domain has approximately 362240 nodes. This value fluctuates for every turbine and geometrical model, but the pre-set is the same for every evaluation. To further increase the quality of the results, an inflation layer was generated for the blades of the turbine, further diminishing the size of the mesh and gaining precision in the calculation.
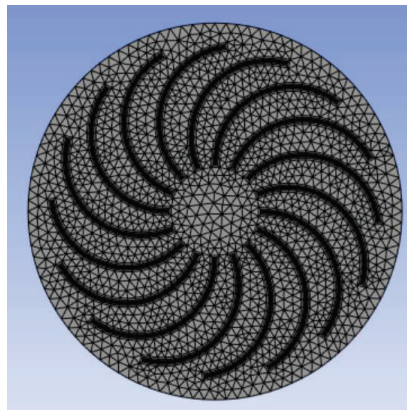

Figure. 6. *Mesh of tetrahedral elements over the turbine.*

As a final step previous running the simulations a time step must be defined. To avoid long computational processes and according to Tourdarbi et al. [20], a series of time steps must be defined as a translation of angle: $\Delta\theta = 1°$, $\Delta\theta = 0.5°$ or $\Delta\theta = 0.25°$. This is translated into the simulation as a time step of 0.005 s [20]. Another parameter for the simulation is limiting the number of iterations to 50 which allows the solver to converge into a result.

4.3.3. Simulation results and final selection

CFD simulations were carried out for the 18 generated models, and the graphical results obtained for the TS-01 simulation are shown in Figure 7.
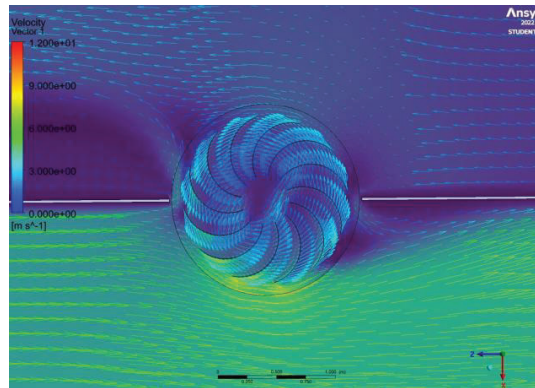

Figure. 7. Velocity and vector contour for TS-01 model.

Reports were generated for all simulations for the analysis of the relevant parameters in MatLab. The speed of the turbine's tip was obtained through CFD and the no-slip boundary condition, while the moment was obtained through FEA (Finite element analysis). From these simulations, TSR, C_t, and C_p were calculated with the assistance of Eq. (1) and Eq. (2).

The turbines were grouped by attack angle to show the graphed results in Figure 8 and Figure 9. The maximum C_p value of the 6° angle group was obtained with TS05 at 0.0594 and a TSR of 0.2456. In the group of 10° angle, the maximum C_p was 0.5686 from TS07 and a TSR of 0.2903 and from the 14° angle group the maximum C_p was 0.0583 with a TSR of 0.3094 corresponding to TS13. Overall, the C_p and C_t values show low efficiency, but high starting torque, which is a good value for the current wind resource measured in-site. The generated vortices in the turbine show unbalance and indicate the need for higher structural resistance. The crossflow functionally of the turbine is neglected and instead, the re-entry angle becomes sharper, inducing a lower efficiency of the turbine.
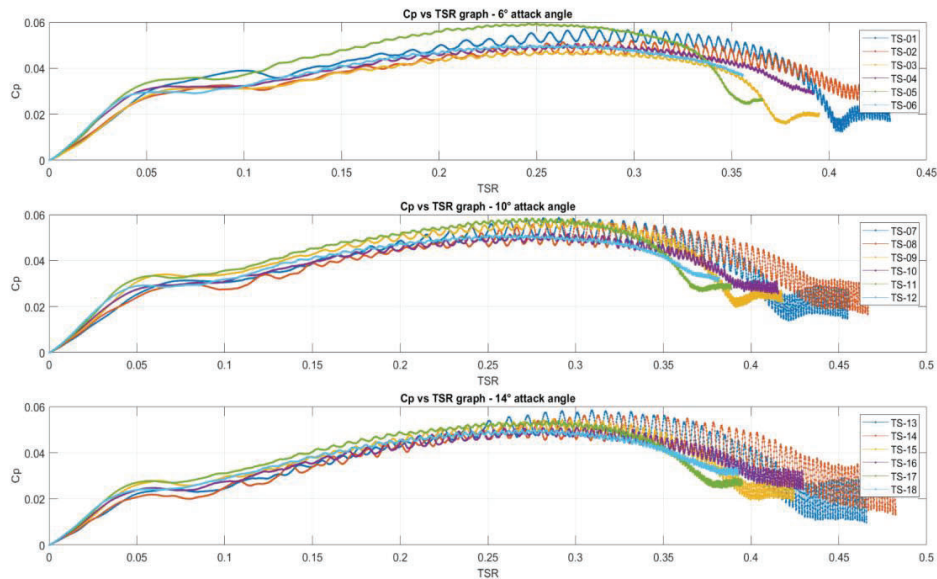

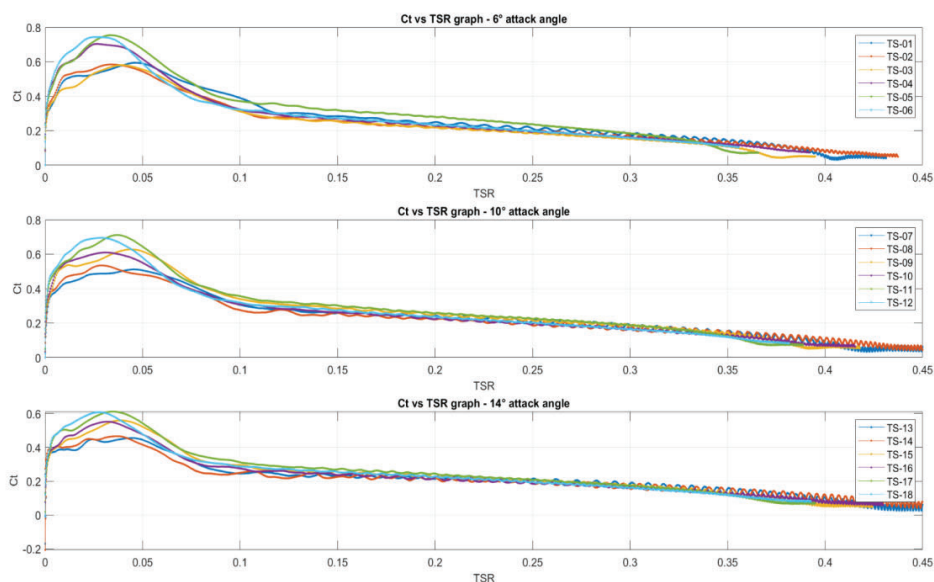*Figure. 8. Resultant C_p vs TSR plot grouped by attack angle.*

Figure. 9. Resultant C_t *vs TSR plot grouped by attack angle.*

From all these values a multivariate statistical analysis was carried out with C_p and their related TSR. The data input is given in Table 4. The software STATGRAPHICS 19 Centurion was used to carry out the multivariate analysis.

Table 4. *Data for factorial analysis.*

Part name	Angle of attack α_1	Number of blades	Height, m	C_p	TSR
TS-01	6°	12	0.9	0.0570	0.2742
TS-02	6°	12	1.1	0.0520	0.3161
TS-03	6°	16	0.9	0.0474	0.2456
TS-04	6°	16	1.1	0.0505	0.2701
TS-05	6°	20	0.9	0.0594	0.2456
TS-06	6°	20	1.1	0.0500	0.2639
TS-07	10°	12	0.9	0.0586	0.2903
TS-08	10°	12	1.1	0.0566	0.3002
TS-09	10°	16	0.9	0.0580	0.2973
TS-10	10°	16	1.1	0.0518	0.2868
TS-11	10°	20	0.9	0.0583	0.2755
TS-12	10°	20	1.1	0.0511	0.2542
TS-13	14°	12	0.9	0.0583	0.3094
TS-14	14°	12	1.1	0.0564	0.3202
TS-15	14°	16	0.9	0.0545	0.2871
TS-16	14°	16	1.1	0.0512	0.3006
TS-17	14°	20	0.9	0.0537	0.2834
TS-18	14°	20	1.1	0.0502	0.2763

The first conducted analysis was the optimization for C_p, where the desired behaviour is to maximise this value. Table 5 summarises the obtained values and optimization results. The optimal geometrical properties for energy production were found to be an angle of attack of 11.5495°, a minimum height of 0.9 m and a number of blades of 12.0058, resulting in a C_p prediction of 0.05944. Although the recorded values are low for the given wind speed, this behaviour may be expected due to the lower air density and the definition of TSR and C_p, where the global speed is considered to be the sum of each lane's speed. The surface plot resembles a saddle-back, indicating that higher C_p values may exist on the extreme ends of the number of blades and near 10° attack angle.

Table 5. Optimization results for C_p.

Factor	Lower limit	Upper limit	Optimum value
Angle of attack α_1	6°	14°	11.5495°
Number of blades	12	20	12.0058
Height, m	0.9	1.1	0.9

After obtaining the C_p analysis, a similar analysis was performed for TSR, trying to minimise this value due to the low wind speed present in the selected location. This analysis didn't provide any interesting results. So, an additional analysis was carried out considering both responses. Table 6 shows the resultant values to minimise the TSR and maximise the C_p. The height is the same as for the optimal results in Table 5, but the condition to minimise TSR imposes a higher blade number of blades and lower attack angle, obtaining the value of 20 and 6.4656° respectively. From the response analysis, the predicted C_p is 0.05725 and a TSR of 0.49881.

Table 6. Optimization results for multiresponse analysis.

Factor	Lower limit	Upper limit	Optimum value
Angle of attack α_1	6°	14°	6.46562°
Number of blades	12	20	20
Height, m	0.9	1.1	0.90075

Figure 10 shows the response surface and has a similar shape as the one generated for C_p, but shifted to benefit higher blade numbers and with a sharper slope. The resultant height is the mean between both values, upper and lower limit. This is the default option from the software to avoid dependence of the third variable and since the response from the height is not significant the figure is valid and represents the correct behaviour of the system.
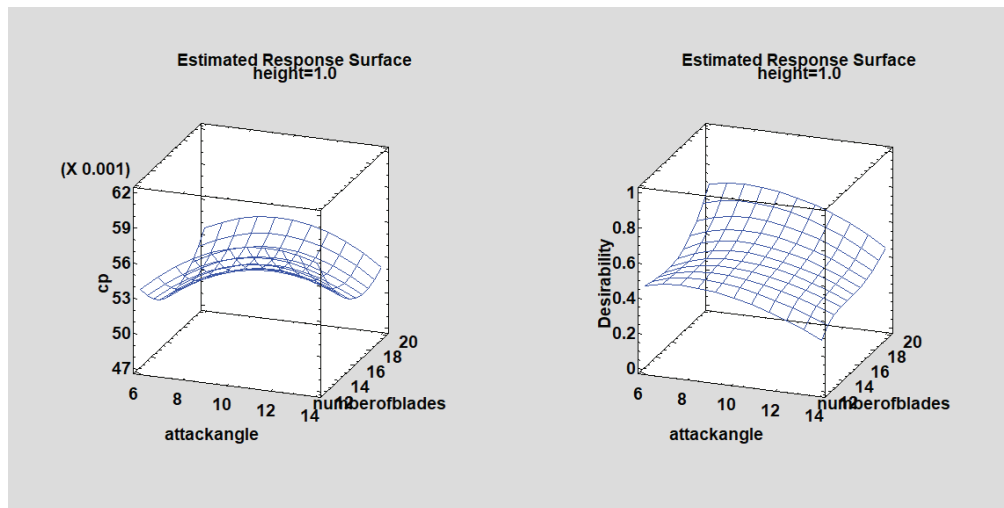

Figure. 10. Estimated response surface for C_p optimization and Multiresponse analysis at height 1 m.

5. Conclusions and recommendations

The design and simulation of a Banki cross-flow wind turbine for highways under high turbulence and high altitude conditions was developed in this work. The results include the following conclusions:

- The number of blades, attack angle and height were optimized for maximum energy production. The results indicate that the number of blades should be 12 and the attack angle and height should be 11.55° and 0.9, respectively.
- The predicted maximum C_p value is 0.05944, which indicates low efficiency. Results that could be improved with the addition of concentrators. The TSR value for this maximum C_p must be minimised to improve turbine performance at lower wind speeds, which is important considering the location and high altitude conditions.
- The optimal value for the combination of the Cp and TSR fluctuates in terms of blade numbers, where higher values indicate higher starting torque and lower self-start speed of the turbine, resulting in a higher Cp shortly after the turbine's cut-in speed. The predicted C_p, in this case is 0.05735 and the optimal blade number is 20 and 6.46° angle.

- The attack angle seems to have a maximum efficiency point for the conditions where the most beneficial angle for energy production appears to be in the middle of the considered parameters. Overall and considering that the difference between C_p's in both analysis is low, the optimal geometrical designs for the turbine are the ones related to the C_p analysis.

The design of the turbine was successful and has a similar approach to other authors in the literature regarding limitations and parametrical design. Nevertheless, we have some recommendations and future work to do:

- The results must be improved with better instruments of measurement and larger intervals of wind speed measurements in order to obtain a more accurate prediction of the resource and to assess the feasibility of installing the turbine over the Blanco Galindo highway.

- The construction of a prototype is also recommended. The prototype should be made from a durable material with a high Young modulus that will enable the turbine to operate correctly. Composite materials offer an advantage in this regard.

- Also, in order to increase the reliability of the study a more realistic CFD analysis should be carried out taking into account the aerodynamics of a moving vehicle, with a higher number of elements and better-quality meshing for a group of turbines (energy harvesting). Moreover, future studies could also consider wind deflectors or other passive elements to increase turbine efficiency.

It is also important to mention that the next steps in this work include manufacturing a couple of prototypes to validate their performance in different conditions and to gather information from at least two sites where the altitude is a predominant factor for eolic generation efficiency. The construction and manufacturing of these prototypes would involve a improvement on Bolivia's renewable energy matrix and distributed generation. The sites chosen for the next stage of the project are the Blanco Galindo Avenue in Cochabamba, Bolivia (2558 m.a.s.l.) and the El Alto - Mallasilla road in La Paz, Bolivia (3500 m.a.s.l.).

Nomenclature

ρ	air density, kg/m^3
α_1	angle of attack, °
β_1	blade angle, °
δ	degree of curvature, °
D_2	inner diameter, m
r_2	inner radius, m
D_1	outer diameter, m
r_1	outer radius, m
P	output power from the turbine, W
S	projected area of the turbine, m^2
c_p	power coefficient
ρ_b	radius of curvature, m
c_t	thrust coefficient
TSR	tip-speed ratio
V	wind speed, m/s

References

[1]   R. Pramod, G. B. V. Kumar, P. S. S. Harsha, and K. A. U. Kumar, "Design and development of nautilus whorl-wind turbine," *AIP Conf. Proc.*, vol. 1859, 2017, doi: 10.1063/1.4990246.

[2]   T. Q. Le, K. S. Lee, J. S. Park, and J. H. Ko, "Flow-driven rotor simulation of vertical axis tidal turbines: A comparison of helical and straight blades," *Int. J. Nav. Archit. Ocean Eng.*, vol. 6, no. 2, pp. 257–268, 2014, doi: 10.2478/IJNAOE-2013-0177.

[3]   J. Blanco, J. de D. Rodriguez, A. Couce, and M. I. Lamas, "Proposal of a nature-inspired shape for a vertical axis wind turbine and comparison of its performance with a semicircular blade profile," *Appl. Sci.*, vol. 11, no. 13, 2021, doi: 10.3390/app11136198.

[4]   R. D. Maldonado *et al.*, "Design, simulation and construction of a Savonius wind rotor for subsidized houses in Mexico," *Energy Procedia*, vol. 57, pp. 691–697, 2014, doi: 10.1016/j.egypro.2014.10.224.

[5]   W. Tian, Z. Mao, X. An, B. Zhang, and H. Wen, "Numerical study of energy recovery from the wakes of moving vehicles on highways by using a vertical axis wind turbine," *Energy*, vol. 141, pp. 715–728, 2017, doi: 10.1016/j.energy.2017.07.172.

[6]   W. Tian, B. Song, and Z. Mao, "Numerical investigation of wind turbines and turbine arrays on highways," *Renew. Energy*, vol. 147, pp. 384–398, 2020, doi: 10.1016/j.renene.2019.08.123.

[7]   I. D. Brownstein, N. J. Wei, and J. O. Dabiri, "Aerodynamically Interacting Vertical-Axis Wind Turbines:

Performance Enhancement and Three-Dimensional Flow," *Energies*, vol. 12, no. 14, p. 2724, 2019, doi: 10.3390/en12142724.

[8] J. Durkacz *et al.*, "CFD modelling and prototype testing of a Vertical Axis Wind Turbines in planetary cluster formation," *Energy Reports*, vol. 7, pp. 119–126, 2021, doi: 10.1016/j.egyr.2021.06.019.

[9] A. H. Rajpar, I. Ali, A. E. Eladwi, and M. B. A. Bashir, "Recent development in the design of wind deflectors for vertical axis wind turbine: A review," *Energies*, vol. 14, no. 16, 2021, doi: 10.3390/en14165140.

[10] E. M. Alave-Vargas, R. Orellana Lafuente, and D. F. Sempértegui-Tapia, "ESTADO DEL ARTE SOBRE AEROGENERADORES DE EJE VERTICAL (Monografía)," *Investig. Desarro.*, vol. 22, no. 1, pp. 161–172, 2022, doi: 10.23881/idupbo.022.1-13i.

[11] A. A. Al-Maaitah, "The design of the Banki wind turbine and its testing in real wind conditions," *Renew. Energy*, vol. 3, no. 6–7, pp. 781–786, 1993, doi: 10.1016/0960-1481(93)90085-U.

[12] F. Alqurashi and M. H. Mohamed, "Aerodynamic forces affecting the H-rotor darrieus wind turbine," *Model. Simul. Eng.*, vol. 2020, 2020, doi: 10.1155/2020/1368369.

[13] T. A. Ismaeel, S. Aljabair, O. A. Abdulrazzaq, and Y. A. Abood, "Energy recovery of moving vehicles' wakes in highways by vertical axis wind turbines," *FME Trans.*, vol. 48, no. 3, pp. 557–565, 2020, doi: 10.5937/fme2003557I.

[14] W. YAMAZAKI and Y. ARAKAWA, "Inexpensive airfoil shape optimization for vertical axis wind turbine and its validation," *J. Fluid Sci. Technol.*, vol. 10, no. 2, pp. JFST0015–JFST0015, 2015, doi: 10.1299/jfst.2015jfst0015.

[15] J. J. N. Quispe, J. H. Nina, and S. T. Jara, "Study and application of wind rose for vertical and horizontal axis wind turbine installation in Lima," *Proc. 2020 IEEE Eng. Int. Res. Conf. EIRCON 2020*, pp. 16–19, 2020, doi: 10.1109/EIRCON51178.2020.9254076.

[16] I. J. T. Matias, L. A. M. Danao, and B. E. Abuan, "Numerical investigation on the effects of varying the arc length of a windshield on the performance of a highway installed Banki wind turbine," *Fluids*, vol. 6, no. 8, 2021, doi: 10.3390/FLUIDS6080285.

[17] V. Sammartano, C. Aricò, A. Carravetta, O. Fecarotta, and T. Tucciarelli, "Banki-Michell optimal design by computational fluid dynamics testing and hydrodynamic analysis," *Energies*, vol. 6, no. 5, pp. 2362–2385, 2013, doi: 10.3390/en6052362.

[18] A. A. Al-Aqel, B. K. Lim, E. E. M. Noor, T. C. Yap, and S. A. Alkaff, "Potentiality of small wind turbines along highway in Malaysia," *Proc. 2016 Int. Conf. Robot. Autom. Sci. ICORAS 2016*, 2017, doi: 10.1109/ICORAS.2016.7872634.

[19] D. D. D. P. Tjahjana, P. Purbaningrum, S. Hadi, Y. A. Wicaksono, and D. Adiputra, "The study of the influence of the diameter ratio and blade number to the performance of the cross flow wind turbine by using 2D computational fluid dynamics modeling," *AIP Conf. Proc.*, vol. 1931, pp. 2–7, 2018, doi: 10.1063/1.5024093.

[20] S. Toudarbari, M. J. Maghrebi, and A. Hashemzadeh, "Evaluation of Darrieus wind turbine for different highway settings using CFD simulation," *Sustain. Energy Technol. Assessments*, vol. 45, no. November 2020, p. 101077, 2021, doi: 10.1016/j.seta.2021.101077.

[21] S. Singh Rathore, R. Dalmia, K. Tamakuwala, and S. Manavalla, "Design, Fabrication and Testing of a Low Cost Vertical Axis Wind Mill for Low End Power Generation," *Int. Res. J. Eng. Technol.*, pp. 1524–1528, 2016, [Online]. Available: www.irjet.net.

[22] A. R. Gatlewar, N. K. Mandavgade, M. T. Kanojiya, and V. N. Kalbande, "Material selection for rotor blade of vertical axis wind turbine," *Mater. Today Proc.*, vol. 46, no. xxxx, pp. 8489–8493, 2021, doi: 10.1016/j.matpr.2021.03.505.

[23] ISO. 4439:1979, "Unplasticized polyvinyl chloride (PVC) pipes and fittings — Determination and specification of density," 1979. https://www.iso.org/standard/10341.html.

[24] I. Ushiyama, I. Isshiki, and G. Z. Chai, "Experimentally evaluating the design and performance of cross-flow wind rotors," *Energy Environ. into 1990´s*, vol. 3, pp. 1499–1504, 1990.

[25] J. De Andrade, C. Curiel, F. Kenyery, O. Aguilln, A. Vásquez, and M. Asuaje, "Numerical investigation of the internal flow in a Banki turbine," *Int. J. Rotating Mach.*, vol. 2011, 2011, doi: 10.1155/2011/841214.

[26] M. H. Mohamed, A. M. Ali, and A. A. Hafiz, "CFD analysis for H-rotor Darrieus turbine as a low speed wind energy converter," *Eng. Sci. Technol. an Int. J.*, vol. 18, no. 1, pp. 1–13, 2015, doi: 10.1016/j.jestch.2014.08.002.